Research article

Tenability on schiff base Hydrazone derivatives and Frontier molecular orbital

E.H. El-Mossalamy [a], Nouf F. Al-Harby [b,*], S. Abdel Aal [a,b], N.M. Ali [a], M. El-Desawy [c], Mahmoud M. Elewa [d], Mervette El Batouti [e]

[a] Chemistry Department, Faculty of Science, Benha University, Benha, Egypt
[b] Department of Chemistry, College of Science, Qassim University, Buraidah 51452, Saudi Arabia
[c] Nuclear Physics Department, Nuclear Research Centre, AEA, 13759 Cairo, Egypt
[d] Arab Academy for Science, Technology and Maritime Transport, Alexandria P.O. Box 1029, Egypt
[e] Chemistry Department, Faculty of Science, Alexandria University, Alexandria 21526, Egypt

ARTICLE INFO

ABSTRACT

Context hydrazine compounds based on 1,3,5-triazine were synthesised and their molecular structures were characterised by elemental analysis, Electronic, IR and ^{1}H NMR spectra. The spectral behaviour of the newly prepared compounds in organic solvents of different polarities was extensively studied and correlated to the molecular structure. In this study, 1,3,5-Triazine derivatives (L1, L6, L7, L8) have been subjected to theoretical studies using the Semi-empirical PM3 quantum chemical method. The physical-chemical properties of some Hydrazone derivatives are determined theoretically. The molecular geometry, the Highest Occupied Molecular Orbital (HOMO) - Lowest Unoccupied Molecular Orbital (LUMO) energy gap, molecular hardness (η), ionisation energy (IE), Electron affinity and total energy were analysed, and applications as biological effects were done.

1. Introduction

Schiff bases are a class of compounds that arise from the reaction between carbonyl compounds and hydrazine or primary amines, forming azomethine compounds (CH=NH–). These derivatives are highly significant due to their various applications in the fields of biology, medicine, clinical research, pharmacology, and analytical chemistry, as evidenced by numerous studies [1]. Moreover, they are widely favoured as ligand precursors owing to their adaptability and straightforward synthesis. 1,3,5-Triazine is a noteworthy group of organic heteroaromatic compounds that are widely utilised in various designs and applications such as charge transport materials [2], organic light-emitting materials [3], and the creation of organic materials with non-linear optical behaviour. Molecules, metal complexes, and materials based on 1,3,5-triazine have various applications, including catalysis [4], CO_2 gas adsorption [5], and the design of photochromic complexes [6]. Triazine, a nitrogen-containing heterocyclic compound, has garnered significant attention from researchers due to its diverse range of biological properties. These properties include anti-viral, antitumor, anti-convulsant, analgesic, antioxidant, anti-depressant, herbicidal, insecticidal, fungicidal, antibacterial, and anti-inflammatory activities. Researchers have synthesised different antibacterial agents to combat bacterial diseases. However, the emergence of drug resistance, tolerance, and side effects has necessitated the development of a new class of antibacterial agents with enhanced pharmacological

* Corresponding author.
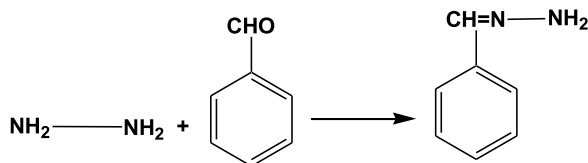E-mail address: hrbien@qu.edu.sa (N.F. Al-Harby).

properties [7,8]. 1,3,5-Triazine derivatives, also called s-triazine, have been known [9–12] for a long period. Scientists have found widespread applications in the pharmaceutical, textile, plastic, and rubber industries, and are used as pesticides, dyestuffs, optical bleaches, explosives, and surface-active agents. These compounds are also recognised as powerful chelating agents, which can be used as liquid crystals, metal complexes, and new hydrogenation catalysts.

The decision to explore 1,3,5-triazine in the development of 1,3,5-triazine derivatives is based on the fact that the triazine ring has a deficiency of π-electrons. This allows it to function as an electron acceptor in the molecular structure. The π-electrons in the ring are partially localised on the nitrogen atoms, while the carbon atoms have a lower electronic charge. Additionally, due to this phenomenon, the 2nd, 4th, and 6th positions of the triazine ring are susceptible to nucleophilic attack from appropriate nucleophiles. This characteristic enhances the synthetic approaches for creating 1,3,5-triazine derivatives [13]. Recently, there has been ongoing research into the development and production of 1,3,5-triazines and their derivatives. This is because these compounds possess interesting properties such as molecular symmetry and electronic characteristics [3–6].

The molecular orbital computations (MOC) is an aspect of chemistry that is fast spreading and has become a useful tool in studying molecular systems prior to synthesizing the system in the laboratory. It has also aided in our understanding of biochemical processes such as enzymatic reactions, and photosynthesis, it assisted in the design of new drugs and chemical compounds in general with specific properties and led to the discovery of structure–property–reactivity relationships. Semi-empirical PM3 calculations have been the best in predicting transition and organometallic metal complexes' geometric properties and vibrational frequencies [10]. Computer simulation analysis necessitates a dynamic viewpoint to account for the incessantly fluctuating elements. The precision of instruments, experimental methodologies, and computational capabilities and efficiency are continuously advancing. Recent advancements in mathematics and algorithms have led to improved dependability and precision of outcomes in contrast to experimental methods. Ab initio and DFT techniques are capable of accurately investigating larger systems, however, there exist numerous intriguing molecular systems that necessitate the utilisation of semi-empirical methods for their study. Semi-empirical methods like PM3 are advantageous in quantum chemistry due to their high generality, accuracy, and low computational cost. This makes them particularly valuable for studying intricate molecular systems. Ab initio and DFT predominantly utilise deductive approaches, whereas semi-empirical methods employ inductive approaches to expedite computations. Computer simulations possess a unique research methodology by combining different strategies in varying proportions to facilitate the acquisition of new knowledge [14].

This activity is attributed to the formation of stable chelate complexes with transition metals which catalyse physiological processes [11]. They also act as herbicides, insecticides, nematicides, rodenticides, plant growth regulators, and sterilant for houseflies, among other applications [12,15]. In analytical chemistry, hydrazones find applications as multidentate ligands for transition metals in calorimetric or fluorometric determinations [16,17].

Schiff bases [18,19] were still regarded as one of the most potential groups of organic compounds for facile preparations of metallo-organic hybrid materials. In the past two decades, the properties of Schiff base stimulated much interest for their noteworthy contributions to single molecule-based magnetism; material science, the interest in Schiff base compounds as analytical reagents is increasing since they enable simple and inexpensive determinations of different organic and inorganic substances [20]. In This study, we report the molecular geometry, HOMO-LUMO energy gap, molecular hardness (η), ionization energy (IE), electron affinity (EA), and total energy of L1, L6, L7 and L8 compounds supported by semi-empirical calculations, and applications as biological effect done.

2. Experimental

2.1. Materials

All reagents used in the present study were of the highest quality (Merck, Aldrich, Fluka and Sigma Research Laboratories) and were used without further purification. Freshly bi-distilled water was used whenever water was necessary.

Preparation of the organic ligands:

The hydrazones under study were prepared via three steps, firstly, the Preparation of 4-amino-6-phenylamino- [1,3,5]triazine-2-carboxylic acid ethyl ester (S1) by condensation of phenylbiguanide (I) with diethyloxalate (II), as follows.

I   II   Ester 4-Amino-6-phenylamino-

[1,3,5]triazine-2-carboxylic acid ethyl S1

Condensation of phenylbiguanide (I) with diethyloxalate (II).

Secondly, the Preparation of hydrazine derivatives (S2) by condensation of hydrazine hydrate with aldehyde derivatives (Benzaldehyde, 2H- pyrrole-2-carboxaldehyde, 1-Pyridine-2-yl-ethanone, 3,4-dihydro-2H-naphthalene-1-one, 1-phenyl ethanone, 4-chloro-benzaldehyde, 4-hydroxy-benzaldehyde, and 4-amino-benzaldehyde) which can be represented by the following reaction (as

one derivative).

(S2)

Preparation of hydrazine derivatives (S2).

Thirdly, the Preparation of the hydrazones (I -VIII) by the reaction of hydrazones with 4-amino-6-phenylamino- [1,3,5]tri-azine-2-carboxylic acid ethyl ester (S1). The prepared Hydrazones have the following structures in Scheme 1.

First, the prepared organic compound's purity was confirmed by melting point constancy. Elemental analysis data (Table 1) show satisfactory agreement with the expected tentative formulae.

2.2. Physical measurements

2.2.1. Elemental analysis

Elemental analysis of (C, H, N) elements was carried out on 2400II CHN analyser with acetanilide as the standard material and given in Table 1.

2.2.2. ^1H NMR spectra

Proton Nuclear Magnetic Resonance (^1H NMR) spectroscopy is a highly effective analytical method employed in chemistry for elucidating the structure of organic compounds. It offers data regarding the quantity of hydrogen atoms in a molecule, their electronic surroundings, and their interconnections. The following are the main characteristics of ^1H NMR spectroscopy: Chemical Shift (δ) is the displacement of a nuclear magnetic resonance (NMR) signal in a molecule's spectrum, relative to a reference compound, due to the influence of its chemical environment. Chemical shift refers to the frequency at which a nucleus resonates compared to a standard in a magnetic field. The measurement is denoted in units of parts per million (ppm). Current patterns or tendencies: Electronegative groups near a hydrogen atom cause it to become less shielded, leading to a shift towards higher ppm values. The chemical shifts of hydrogens on sp3 carbons generally range from 0.5 to 4 ppm, while those on sp2 carbons typically fall between 4 and 6 ppm. Hydrogens on sp carbons, on the other hand, tend to appear at chemical shifts of 6–8 ppm. The chemical shifts of the hydrogen atoms in aromatic compounds typically range from 6 to 8.5 ppm. Coupling: The hydrogens on adjacent carbons can interact, resulting in the division of NMR signals. The value of n incremented by 1. Principle: When a hydrogen atom is surrounded by n identical neighbouring hydrogens, it will produce a spectrum with n+1 distinct peaks. Patterns such as doublets, triplets, quartets, and more intricate arrangements can be observed, providing insight into the interconnectedness of atoms. The integral of each NMR signal is directly proportional to the quantity of hydrogen atoms that contribute to that signal. This is utilised to ascertain the relative abundance of distinct hydrogen atom variants within the molecule. The term "multiplicity" refers to the state or condition of having multiple or many instances, elements, or aspects. Singlet: A peak without any splitting, indicating the absence of adjacent hydrogens. Doublet, Triplet, Quartet, etc. refer to groups of two, three, or four, etc. items or individuals. Representative of adjacent hydrogens numbered 1, 2, 3, etc. Alkyl groups (R–CH3, R–CH2-R) are usually found in the range of 0.5–2 ppm. The chemical shifts of allylic and benzylic hydrogens typically range from 2 to 3 ppm. Alkenes exhibit chemical shifts in the range of approximately 4.5–6.5 parts per million (ppm). The chemical shifts of aromatic hydrogens typically range from 6 to 8.5 ppm. The concentration of aldehydes is approximately 9–10 parts per million (ppm). Carboxylic acids exhibit chemical shifts in the range of approximately 10.5–12 parts per million (ppm). The selection of solvent can
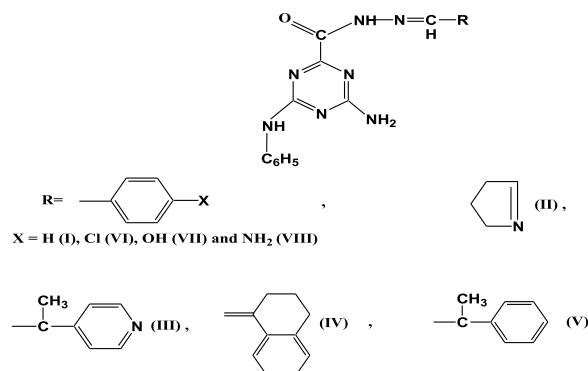
Scheme 1. Preparation of the hydrazones (I -VIII).

Table 1
Elemental analysis data and tentative formula for the ligands under Investigation.

Ligand	Empirical formula	Molecular weight	Microanalysis Calc. (Found)					M.P. (°C)	Colour
			%C	%H	%N	%O	%Cl		
I	$C_{17}H_{15}N_7O$	333.35	61.25 (61.32)	4.54 (4.43)	29.41 (29.45)	4.80 (4.80)	–	148–150	Yellow
II	$C_{15}H_{14}N_8O$	322.32	55.89 (55.36)	4.38 (5.25)	34.76 (34.97)	4.96 (4.42)	–	160–162	Yellowish-brown
III	$C_{17}H_{16}N_8O$	348.36	58.61 (58.62)	4.63 (4.62)	32.17 (32.19)	4.59 (4.57)	–	336–338	Yellowish white
IV	$C_{20}H_{19}N_7O$	373.41	64.33 (64.36)	5.13 (5.15)	26.26 (26.21)	4.28 (4.28)	–	180–182	Buff
V	$C_{18}H_{17}N_7O$	347.37	62.24 (62.61)	4.93 (4.62)	28.23 (28.26)	4.61 (4.51)	–	124–126	Yellow
VI	$C_{17}H_{14}ClN_7O$	367.79	55.51 (55.07)	3.84 (3.67)	26.66 (26.69)	4.35 (4.36)	9.64 (10.21)	210–212	Yellowish white
VII	$C_{17}H_{15}N_7O_2$	349.35	58.45 (57.95)	4.33 (4.66)	28.07 (27.91)	9.15 (9.48)	–	276–278	Pale yellow
VIII	$C_{17}H_{16}N_8O$	348.36	58.61 (58.41)	4.63 (4.30)	32.17 (32.24)	4.59 (5.05)	–	264–266	Bright Yellow

influence the chemical shifts. Deuterated solvents, such as DMSO and CDCl₃, are employed to mitigate the presence of hydrogen in the solvent, thereby preventing any interference.

^{1}H NMR spectra were recorded using Gemini–200 spectrometer using d⁶-dimethyl sulfoxide (DMSO) as a solvent and tetramethyl silane (TMS) as an internal standard.

2.2.3. Infrared spectra

Infrared (IR) spectroscopy is a potent technique for discerning functional groups in organic compounds, including ligands. Every bond and functional group in a molecule possess a distinctive infrared absorption frequency, usually expressed in wavenumbers (cm^{-1}). Infrared spectra offer insights into the vibrational modes exhibited by functional groups present in a molecule. The fingerprint region, spanning from 1200 to 700 cm^{-1}, exhibits multiple absorption bands associated with C–O, C–C, and C–N single bond stretches, C–H bending vibrations, and benzene rings. The IR spectra were recorded as the KBr disc technique. The percentage transmittance was automatically registered against wave number (cm^{-1}) using a Beckman IR 4280 double-beam spectrophotometer in the frequency range of 4000–200 cm^{-1}.

2.3. Electronic absorption spectra studies of ligands

2.3.1. Spectra in solvents

The solvents used were of spectrophotometric grade. The effect of organic solvent on the electronic absorption spectra of the ligands was studied by measuring the absorption spectra of 1×10^{-5} M solution of each ligand dissolved in the solvent against a blank solution of the same solvent.

Table 2
Characteristic IR frequencies (cm^{-1}) of ligands I-VIII

Ligand	I	II	III	IV	V	VI	VII	VIII
υ_{NH2}	3401	3211	3352	3324	3340	3335	3309	3325
δ_{NH2}	1651	1634	1645	1646	1651	1630	1620	1601
υ_{NH}	3202	3106	3202	3193	3199	3197	3197	3192
δ_{NH}	1492	1495	1494	1493	1494	1491	1498	1493
$\upsilon_{NH-C=O}$	1617	1630	1645	1633	1639	1634	1602	1610
$\upsilon_{C=N}$	1532	1535	1599	1596	1599	1532	1529	1565
$\upsilon_{5H\ adj.}$	752	–	–	–	759	–	–	–
$\upsilon_{2H\ adj}$	–	–	–	–	–	862	824	865
$\upsilon_{CH-phenyl}$	3047	3010	2944	3058	3053	3048	2944	2914
$\upsilon_{CH-pyrrol}$	–	3064	–	–	–	–	–	–
$\delta_{CH\ -pyridine}$	–	–	1640	–	–	–	–	–
υ_{Cl}	–	–	–	–	–	1119	–	–
υ_{OH}	–	–	–	–	–	–	3482	–
δ_{OH}	–	–	–	–	–	–	1628	–
$\upsilon_{sym.-triazine}$	1531	1532	1530	1531	1531	1532	1529	1529
υ_{CH3}	–	–	2955	–	2950	–	–	–
$\upsilon_{CH=N}$	3047	2983	–	–	–	3048	2944	2914
υ_{CH2}	–	2863	–	–	–	–	–	–
υ_{CH}	2947	2976	2832	2938	2959	2938	2861	2840

2.4. Computational methods

Molecular Orbital Computations (MOC) employ sophisticated quantum chemical techniques to calculate the electronic configuration of molecules. These calculations are crucial for predicting a diverse range of chemical properties and behaviour [21]. The MOC was performed using semi-empirical molecular orbital calculation. The method used in these computations is the parametric method (PM3) described by Stewart [22]. The geometric of all stable species studied were completely optimized with respect to all geometrical variables using the EF routine (Eigenvector following) [23]. The program is running under the molecular orbital computations package MOPAC2012 by Stewart [24] for microcomputers.

3. Results and discussions

3.1. IR spectra

The infrared spectrum is known to be one of the most powerful tools that give structural information about the molecule. In the present work, the assignment of the IR absorption bands is carried out by a method suggested by Looker [25,26] according to which the spectrum is subdivided into some regions, namely: the 4000-2600, 1700-1500 and 1000-625 cm^{-1}. The bands corresponding to the vibrations of the aromatic rings were assigned according to the method of Katritziky [27] on substituted benzene.

The infrared spectra of the ligands (I–VIII) given in Table 2 show a medium-intensity band appearing at 3401–3211 cm^{-1} and 3202–3106 cm^{-1} corresponding to the stretching vibrations of NH$_2$ and NH groups, respectively.

3.2. ^{1}H NMR spectra

The ^{1}H NMR chemical shifts (δ; ppm) of the different types of protons expected for the newly prepared ligands, recorded in DMSO-d_6 as a solvent and given in Table 3 are discussed and explained about their molecular structure. Inspection of the ^{1}H NMR spectra shows the following:

The protons of the azomethine group (–CH=N–N–) appear as a singlet signal in the range ($\delta = 9.714$–9.719 ppm) [25]. (1) The signal appearing at $\delta = 3.8$ ppm (s, 1H) is due to the proton of the NH [28,29] group attached to the benzene ring. In compounds I, II, IV and VIII. This signal appears as a broad weak one which is probably due to the involvement of the NH group in hydrogen bonding making the signal very broad to a degree that it couldn't be detected clearly [24]. (2) The triplet signals (t, 2H) present in the ^{1}H NMR spectrum of all ligands within the range ($\delta = 6.1$–7 ppm) are due to the protons of the NH$_2$ group. (3) The singlet signal (s, 3H) present within the range ($\delta = 2.1$–2.3 ppm) in the spectra of ligands III and V is due to the protons of the CH$_3$ group in the phenyl moiety of these two ligands. (4) The signal laying at the very downfield side ($\delta = 10.1$ ppm) for ligand VII is due to the hydrogen of the OH group attached to the phenyl ring and this broadness is due to the hydrogen bond [30]. (5) In ligand II the signals within the range ($\delta = 6.172$–6.709 ppm) due to aromatic protons of the pyrrole ring. Also, in ligand III the signal at 7.8 ppm is due to protons of the pyridine ring. (6) The multiple signals within the range ($\delta = 6.9$–7.8 ppm) in ligands I, V, VI, VII and VIII, are due to the aromatic protons of the phenyl ring. While those appearing at ($\delta = 7.2$–7.3 ppm) in the spectrum of compound IV are due to the protons of the phenyl ring of acetophenone. The protons of (CH$_2$) present in this ring appear at ($\delta = 1.79$–2.8 ppm). (7) The ^{1}H NMR spectra of all ligands under investigation show multiple signals within the range ($\delta = 7.2$–8.18 ppm) that are due to the aromatic protons of the phenyl moiety which appear at different positions due to different environments around each proton.

3.3. Electronic absorption spectra

3.3.1. I- absorption spectra in ethanol

The UV–visible spectra of the compounds under investigation are scanned in ethanol within the wavelength range 190–600 nm and given in Fig.(1). The spectra display three absorption bands; the first one (A) in the 208–254 nm range is due to the moderate energy (π–π*) transition corresponding to (^1L_a←^{1}A) state, while the second band (B) laying in the range 260–314 nm range is due to the low energy π–π* transition (^1L_b←^{1}A) state of the aromatic moiety. The absorption band due to the n–π* transition taking place in the C=N and/or the C=O groups which are expected to appear near 260 nm is probably hidden by the intense band of the π–π* transition [31].

Table 3
Chemical shifts (δ; ppm) for the main protons of ligands I–VIII

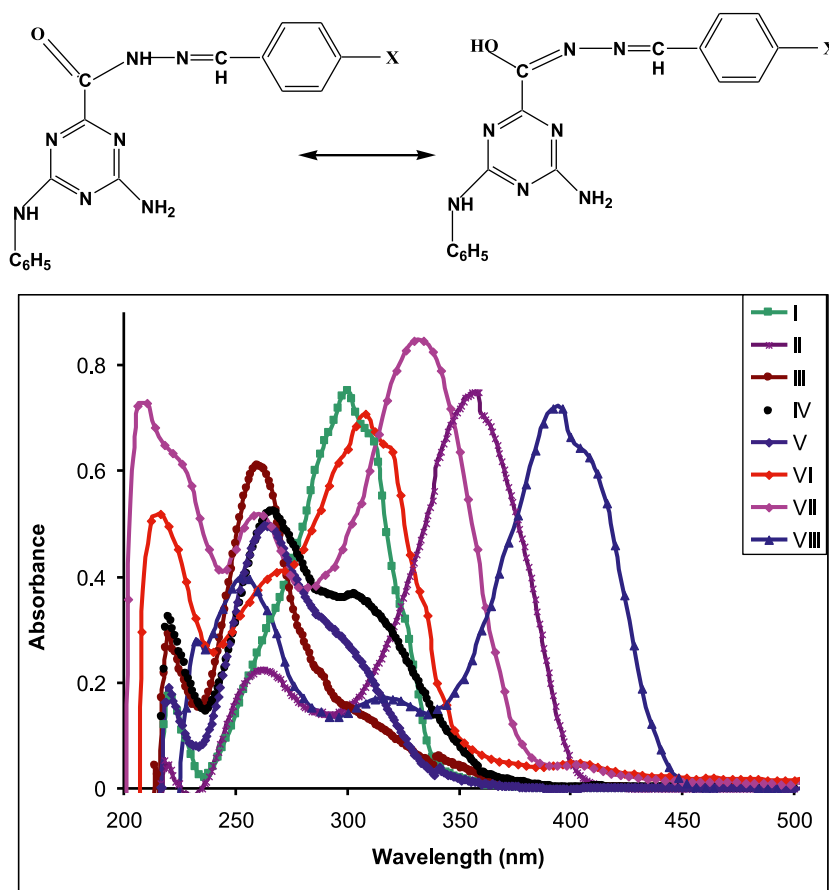| Ligand	1H, –CH=N	1H, –NH	2H, –NH$_2$	3H, –CH$_3$	2H, –CH$_2$	1H, –OH	1H, Pyridine ring	Aromatic Protons of phenyl-C=N	Aromatic protons of phenyl-NH
I	9.72	3.8	6.9–7.01	–	–	–	–	7.21–7.66	7.56–7.9
II	9.72	3.8	6.17–6.25	–	–	–	–	6.17–6.70	7.2–7.3
III	9.72	3.8	6.688	2.11	–	–	7.8	7.81–7.84	7.2–7.3
IV	9.72	–	6.98–7.01	–	1.79–2.8	–	–	7.22–7.36	7.8–8.18
V	9.72	–	6.987	2.3	–	–	–	7.22–7.48	7.8–7.95
VI	9.71	–	6.96–7.01	–	–	–	–	7.22–7.30	7.8–7.91
VII	9.71	–	6.83–6.88	–	–	10.1	–	7.21–7.30	7.7–7.83
VIII	9.71	–	6.74–6.77	–	–	–	–	7.20–7.30	7.6–7.83

Fig. 1. Electronic absorption spectra of Hydrazones in ethanol.

The third band (C) at the longer wavelength side (303–394 nm) is sensitive to the nature of the substituent and is assigned to an electronic transition involving CT interaction within the whole molecule influenced by keto↔enol tautomerism represented as.

3.4. Quantum chemical calculations

The D3 version of Grimme's dispersion, which is currently widely used with higher accuracy, has been utilised to examine the dispersion interaction with the DFT-D3 approach using Gaussian 09 Revision D.01 [19]. The corresponding Gauss View software is used to plot the figures of these complexes. The investigation of non-covalent interactions (NCI) and reduced density gradient (RDG) maps of the examined CT complexes was performed using the Multiwfn analysis program version 3.7 [20] and visualized using Virtual Molecular Dynamics (VMD) [21].

The complete optimization of 1,3,5-Triazine derivatives has been carried out to determine the most stable configurations of examined L1, L6, L7, and L8 CT complexes, as shown in Fig. 2. Intriguingly, the graphical representations of Frontier molecular orbitals (FMOs) including the HOMO and LUMO for the investigated CT complexes in the ground state are performed using the DFT-D3 method along with the 6–311g(d,p) basis set, Fig. 3. As reflected by Fig. 2, the HOMO orbitals of the complexes are mainly distributed over the 4-amino-6-(phenylamino)-1,3,5-triazine-2- carbohydrazide.

(e-donors) whereas, the LUMO orbitals are delocalized over the benzylidene hydrazine (e-acceptors) moiety of the CT complexes, implying the presence of charge transfer along the L1A, L6, L7, and L8 CT complexes. In this context, the observed transitions can be ascribed to n–π* and π–π* transitions, where the n-electrons are localized in the HOMO molecular orbital of the donor. As revealed in Table 4, the decrement in E_{H-L} energy gap for the L6, L7, and L8 concerning L1A suggests a significant enhancement in electrical conductivity, soft and reactive of the target CT complexes, Fig. 4. Obviously, charge-transfer and polarization arise mainly due to the orbital interaction energy of the CT complexes.

Quantum chemical descriptors have been investigated to examine the chemical stability and reactivity of the conjugated structures. The trend in electrophilicity index is as follows: L6 > L1A > L7 >L8, this suggests that the L8 complex is the most reactive among the studied complexes. The chemical potential (μ), which indicates the capacity of electrons in a molecule to escape, is 3.843 eV for the most reactive CT complex (L8) and 4.326 eV for the least reactive CT complex (L6). The extent of electron cloud distortion in an electric
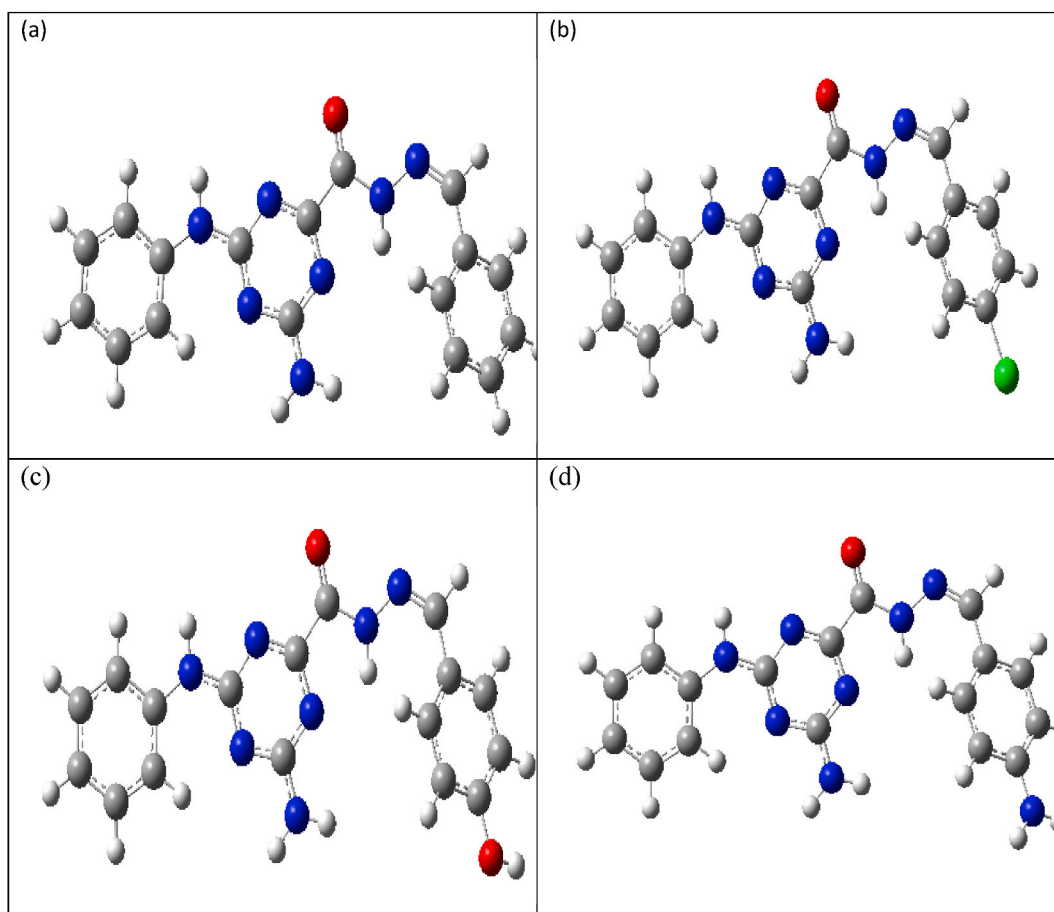
Fig. 2. Optimized structure of (a) L1A, (b) L6, (c) L7, and (d) L8 CT complexes.

field is determined by chemical hardness. In terms of chemical hardness, the examined CT complexes show a sequence of L8 < L6 < L7 < L1A which is consistent with the energy gap, resulting in L8 complex being more reactive. Notably, the lowest ionization potential of the L8 complex (5.632 eV) concerning L1A, L6 and L7 implies the ease of electron transfers through the complex. To gain further insight, the significant decrease in hardness of the L8 (1.789 eV) showed greater reactivity than other examined CT complexes. Noticeably, the given data demonstrate that the electron donor capability (ω^-) values of L1A, L6, L7, and L8 are greater than the electron acceptor capability ω^+ values. The L6, L7 and L8 CT complexes exhibited a smaller chemical hardness η and maximum global softness S values, demonstrating that the CT complexes take place easily with greater efficiency of electron transfer compared to the L1A complex.

To gain further insight into the non-covalent interactions in 1,3,5-Triazine derivatives (L1, L6, L7, and L8) CT complexes. The colour scheme is a red-green-blue scale with red (repulsive) and blue (attractive). The scatter graphs between the reduced density gradient (RDG) and the electron density (ρ) have been depicted in Fig. 4. Green surface corresponds to weak repulsive and weak attractive interactions, respectively. The significant van der Waals interactions, which are weak intermolecular forces, are represented by the green regions near zero between components of the L1, L6, L7, and L8 CT complexes, Fig. 5. This conclusion is in agreement with the geometric analysis, whereby weak interactions are realized between H atom and N atom.

For the non-linear optical (NLO) characteristics of the CT complexes under investigation, there were no experimental standards urea was utilised as a reference pattern in NLO investigations [22,23]. As evidenced in Tables 5 and 6, the L1A, L6, L7, and L8 CT complexes exhibit enhanced polarizabilities to 256.702 a.u., 269.319 a.u., 264.821 a.u., and 301.294 a.u., respectively, concerning 27.857 a.u of urea. The first hyperpolarizability βo increases to 1425.03 a.u., 1622.66 a.u., 1268.67 a.u., and 4613.72 a.u. for the L1A, L6, L7, and L8 CT complexes, respectively. The L1A, L6, L7, and L8 CT complexes are associated with stronger polarizability and first hyperpolarizability, which are dominated by xx and βxxx. the first hyperpolarizability demonstrates a direct correlation between π-conjugation and dipole moment, by Ref. [32]. In particular, the L8 CT complex has the greatest polarizability and first hyper-polarizability, which is approximately 44 times greater than that of urea as the reference material. According to our investigation, the L8 CT complex can be considered as the most candidate for photonic and optical limiting applications owing to the enhancement of its NLO performance and greater response to the external electric field.
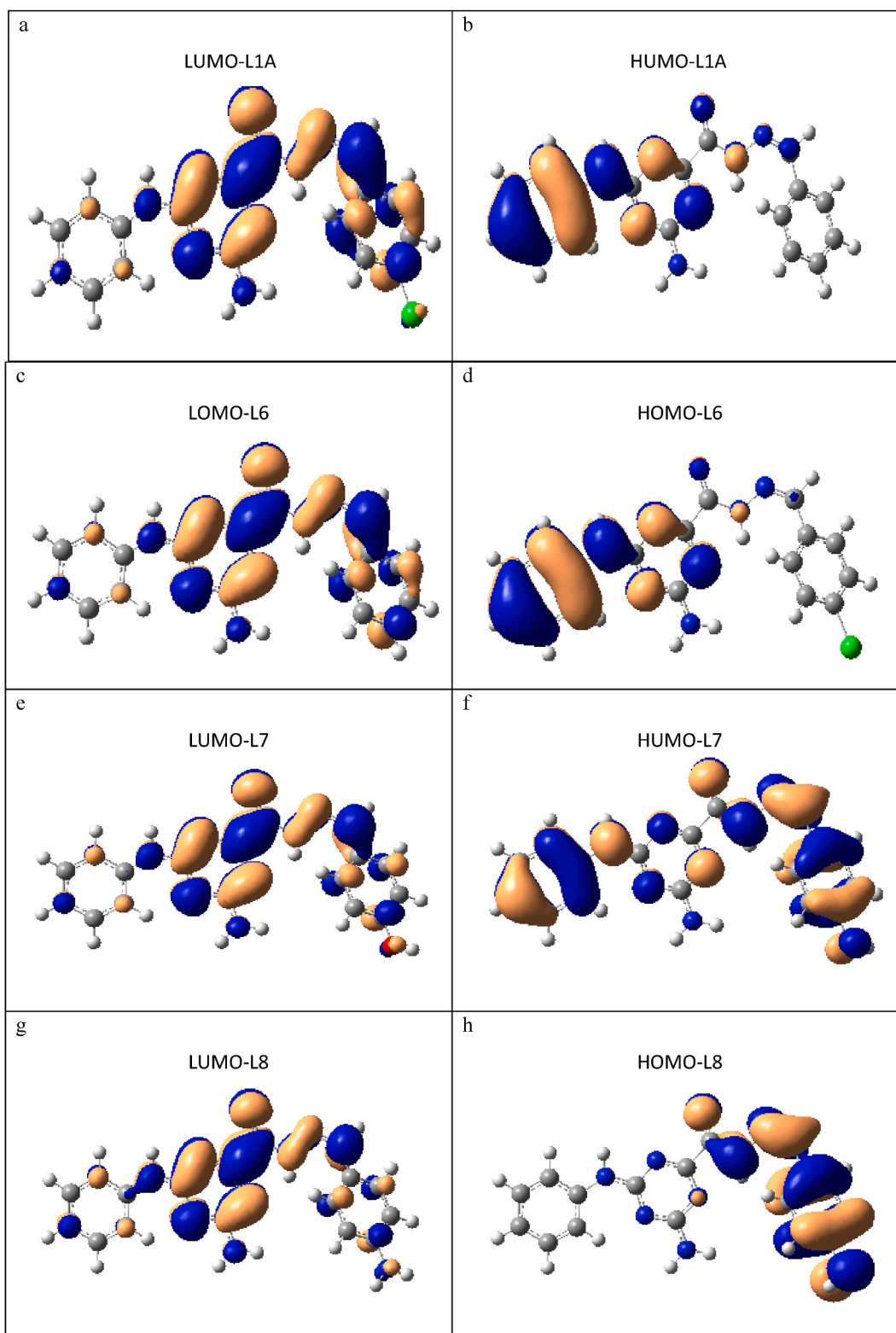
Fig. 3. The LOMO and HUMO states of the most stable configurations of (a, b) L1A, (c, d) L6, (e, f) L7, and (g, h) L8 CT complexes.

Table 4

Frontier molecular orbital energies, HOMO–LUMO energy gap (E_{H-L} gap), ionization energy (IP), electron affinity (EA), chemical potential (μ), electronegativity (χ), global hardness (η), global softness (σ), global electrophilicity (ω), electron donor capability (ω^-), electron acceptor capability (ω^+), and dipole moment of L1A, L6, L7, and L8 CT complexes were calculated using the B3LYP-D3 method along with the SDD basis set.

Energies	L1A	L6	L7	L8
E_{HOMO}	−6.211	−6.276	−6.158	−5.632
E_{LUMO}	−2.242	−2.375	−2.193	−2.054
E_{H-L} gap	3.968	3.901	3.965	3.579
IP = -E_{HOMO}	6.211	6.276	6.158	5.632
EA = -E_{LUMO}	2.242	2.375	2.193	2.054
$\mu = -\left(\frac{I+A}{2}\right)$	−4.227	−4.326	−4.176	−3.843
$\chi = \frac{I+A}{2}$,	4.227	4.326	4.176	3.843
$\eta = \frac{I-A}{2}$)	1.984	1.950	1.982	1.789
$\omega = \frac{\mu^2}{\eta}$)	4.502	4.797	4.398	4.127
$\sigma = \frac{1}{2\eta}$	0.252	0.256	0.252	0.279
ω-	6.863	7.204	6.734	6.272
ω^+	2.636	2.878	2.558	2.429
Dipole moment	7.971	5.886	7.924	10.516
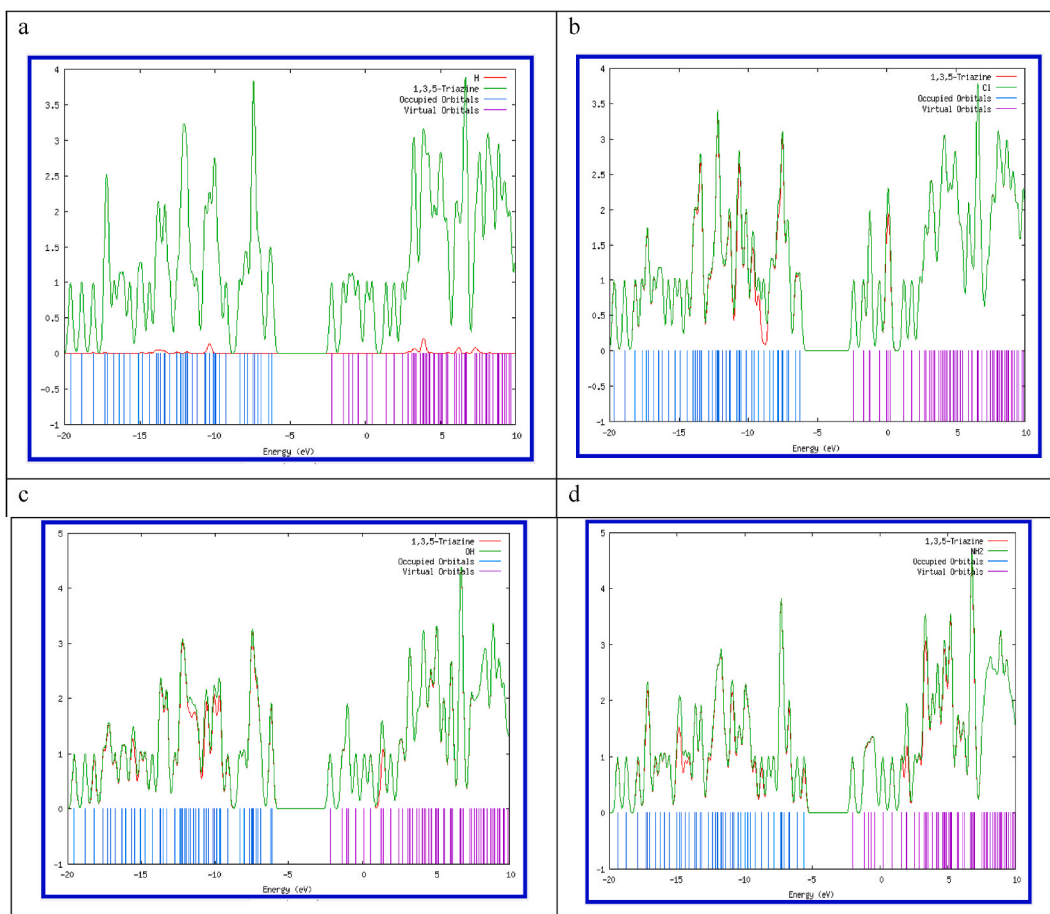
Fig. 4. Partial densities of states (PDOS) of (a) L1A, (b) L6, (c) L7, and (d) L8 CT complexes.
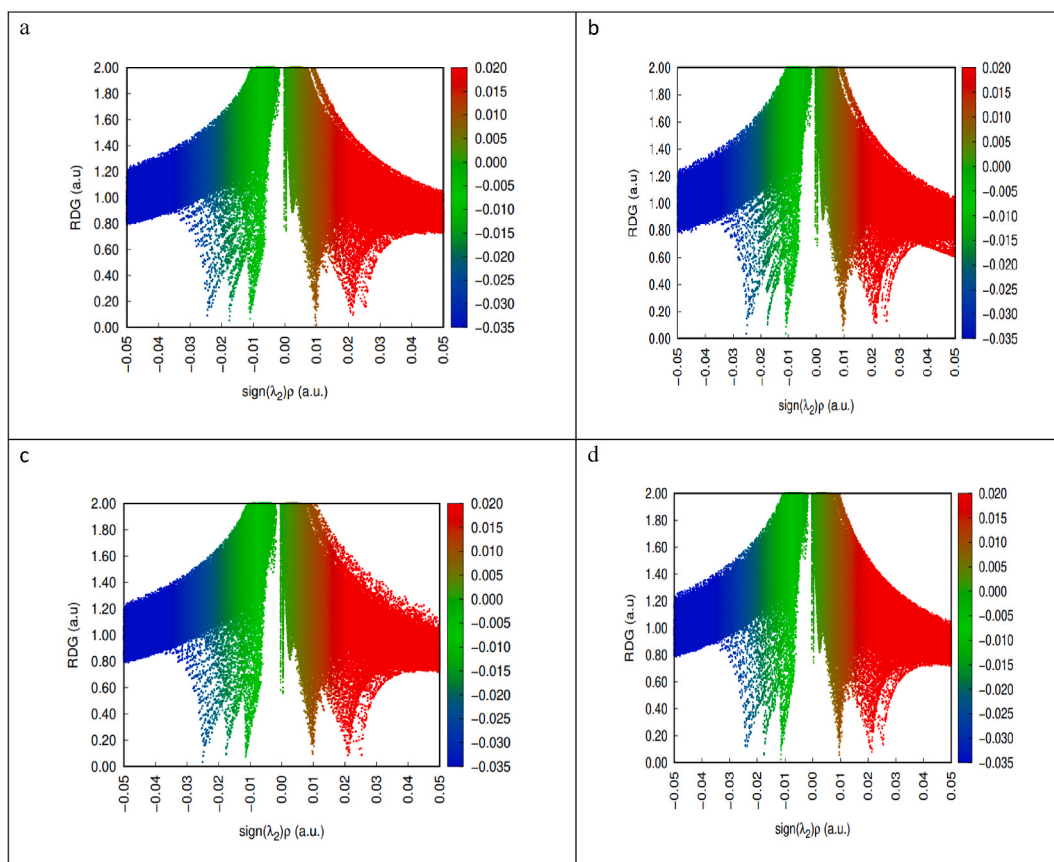
Fig. 5. Reduced density gradient (RDG) of the most stable configurations of (a) L1A, (b) L6, (c) L7, and (d) L8 CT complexes.

Table 5
Polarizabilities (α) of the most stable configuration of urea, L1A, L6, L7, and L8 CT complexes.

System	α_{xx}	α_{xy}	α_{yy}	α_{xz}	α_{yz}	α_{zz}	α	$\Delta\alpha$
Urea	16.535	0.935	33.729	0.00	0.00	33.307	27.857	411.744
L1A	408.301	−27.563	255.917	−21.344	−1.2264	105.889	256.702	102149.8
L6	422.454	−22.3	277.057	−23.683	−0.5745	108.44547	269.319	109247.7
L7	420.623	−26.125	267.021	−22.622	−0.04	106.8201	264.821	109511.2
L8	535.32	−41.46	275.229	0.03354	−0.0185	93.33171	301.294	216625.6

Table 6
First hyperpolarizabilities (βo) of the most stable configuration of urea, L1A, L6, L7, and L8 CT complexes.

System	β_{xxx}	β_{xxy}	β_{xyy}	β_{yyy}	β_{xxz}	β_{xyz}	β_{yyz}	β_{xzz}	β_{yzz}	β_{zzz}	β_{o}
Urea	−9.569	−12.294	−21.821	−101.22	0.00	0.00	-1E^{-07}	−22.467	33.477	0.00	101.676
L1A	1423.43	−148.303	−180.06	67.469	−62.504	−10.817	9.501	13.466	−14.194	1.229	1425.03
L6	1593.4	272.840	−358.78	306.741	−107.57	−19.204	3.202	5.352	7.366	−1.024	1622.66
L7	1162.09	63.716	656.777	−509.00	−0.534	0.320	−0.099	−5.5618	2.698	−0.0037	1268.67
L8	4555.04	−506.072	1037.36	−733.51	3.318	−0.779	0.353	−12.048	6.644	−0.0401	4613.72

3.5. Biological impact

The organic ligands (IV, VII and VIII) were screened in-vitro for their antibacterial activity against gram-positive (Staphylocoeucs aureus) and gram-negative (Escherichia coli) bacterial and fungus (Aspergillus flavus, Candida albicans). Bacterial strains by using the agar diffusion method (15) at a concentration of 0.1 gm/L using nutrient agar as a medium to select the most potent compound and sensitive bacterial species for further investigations. The minimum actual inhibition zone diameter (mm) of the compounds under investigation is collected in Table 7.

Table 7

Minimum actual inhibition zone diameter of organic ligands against Gram-positive and Gram-negative bacteria and fungi.

Ligand	*C.albicans* (fungs)	*A.flavus* (Fungs)	*S. aures* (Gram-positive)	*E. Coli* (Gram-negative)
IV	0.0	0.0	11	13
VII	0.0	0.0	11	12
VIII	0.0	0.0	0.0	11

The data obtained show that the selected compounds are completely inactive against fungi but ligands IV, and VII are completely moderately active against gram-positive and gram-negative bacteria. On the other hand, compound VIII is moderately active against one type of bacteria (Staphylocoeucs aureus) but not active against Staphylocoeucs aureus.

Against all the fungi under study, ligands did not exhibit any remarkable activity compared with bacteria (gram-positive and gram-negative) where all ligands show moderate activity. It is suggested that the ligands having antimicrobial activity may act either by killing the microbe or by inhibiting the multiplication of the microbe by blocking their active sites [16].

The biological impacts of 1,3,5-triazine derivatives (L1A, L6, L7, L8) exhibit variability contingent upon the individual compound. Nevertheless, it has been demonstrated that all four compounds exhibit a certain level of anti-cancer activity in vitro [33,34].

LA has demonstrated efficacy against a diverse range of cancer cell lines, encompassing breast cancer [35], colon cancer, and lung cancer [36]. The mechanism of action is believed to involve the disruption of the cell cycle, leading to the induction of apoptosis in cancer cells.

L6, commonly referred to as atrazine, is an herbicidal substance employed for weed management in diverse crops [37]. Nevertheless, previous studies have demonstrated its in vitro anti-cancer properties. The mechanism of action is believed to involve the selective inhibition of ornithine decarboxylase, a protein that plays a crucial role in the biosynthesis of polyamines. Polyamines play a crucial role in cellular proliferation and mitosis. Consequently, cancer cell growth can be inhibited by specifically targeting ornithine decarboxylase, as demonstrated by the effects of L6 [36].

L7, alternatively referred to as prometryn, is an additional herbicidal agent employed for weed management across diverse crop types. Moreover, it has been demonstrated to exhibit anti-cancer properties in vitro [38]. The mechanism of action is believed to involve the specific targeting of a protein known as topoisomerase II, which plays a crucial role in the process of DNA replication. L7 can induce DNA damage and cellular apoptosis through its specific targeting of topoisomerase II.

L8, alternatively referred to as terbutryn, is an additional herbicidal agent employed for the purpose of weed management across diverse crop species. Furthermore, it has been demonstrated to exhibit anti-cancer properties in vitro. The mechanism of action is believed to involve the selective targeting of tubulin, a protein that plays a crucial role in the process of cell division. The disruption of cell division and subsequent induction of apoptosis in cancer cells can be achieved by specifically targeting tubulin with L8 [39].

Additional investigation is required to ascertain the safety and effectiveness of these substances in the human population. Nevertheless, the findings from in vitro investigations indicate that they possess promising qualities as agents for combating cancer.

4. Conclusions

The potential medicinal and biological significance of Schiff bases is both promising and noteworthy. The investigation of the medicinal properties of Schiff bases necessitates a particular focus in this area.

Schiff bases represent a prominent category of ligands that are commonly synthesised through a straightforward process involving the condensation of a ketone or aldehyde with amines. These substances exhibit a diverse range of biological applications. This study investigates the theoretical properties of 1,3,5-Triazine derivatives (L1, L6, L7, L8) through the application of The D3 version of Grimme's dispersion, which is now prevalent for its enhanced precision, has been employed to investigate the dispersion interaction with the DFT-D3 technique utilising Gaussian 09 Revision D.01. The figures of these complexes are plotted using the associated Gauss View programme. The Multiwfn analysis programme version 3.7 was utilised to investigate the non-covalent interactions (NCI) and reduced density gradient (RDG) maps of the studied CT complexes. The visualisation of these maps was done using Virtual Molecular Dynamics (VMD). Theoretical methods are employed to determine the physical-chemical properties of certain Hydrazone derivatives. The analysis encompassed the examination of molecular geometry, the HOMO-LUMO energy gap, molecular hardness (η), ionisation energy (IE), electron affinity, and total energy. Furthermore, the investigation explored potential applications of these properties concerning the diverse biological applications of Schiff bases. These applications encompass various areas such as antimicrobial activity, plant growth regulation, antioxidant properties, enzymatic functions, anticancer effects, anti-inflammatory properties, anti-malarial activity, antiviral effects, neuroprotective capabilities, analgesic properties, anticonvulsant effects, and neurotoxicity.

Data availability statement

Data will be available upon request.

CRediT authorship contribution statement

E.H. El-Mossalamy: Validation, Supervision, Conceptualization. **Nouf F. Al-Harby:** Writing – review & editing, Investigation, Funding acquisition. **S. Abdel Aal:** Writing – review & editing, Software, Data curation. **N.M. Ali:** Writing – original draft,

Methodology, Formal analysis. **M. El-Desawy:** Resources, Formal analysis, Data curation. **Mahmoud M. Elewa:** Writing – review & editing, Visualization, Resources. **Mervette El Batouti:** Writing – original draft, Supervision, Conceptualization.

Declaration of competing interest

Acknowledgements

References

[1] P. Deshmukh, P.K. Soni, A. Kankoriya, A.K. Halve, R. Dixit, 4-Aminoantipyrine: a significant tool for the synthesis of biologically active Schiff bases and metal complexes, Int. J. Pharm. Sci. Rev. Res. 34 (2015) 162–170.

[2] A. Lorente, P. Pingel, G. Liaptsis, H. Krüger, S. Janietz, Modulation of ambipolar charge transport characteristics in side-chain polystyrenes as host materials for solution processed OLEDs, Org. Electron. 41 (2017) 91–99, https://doi.org/10.1016/j.orgel.2016.11.036.

[3] N. Zhang, Q.-L. Guan, C.-H. Liu, Y. Sun, B. Li, Y.-H. Xing, F.-Y. Bai, A rht-type Luminescent Zn (II)-MOF constructed by triazine hexacarboxylate ligand: tunable luminescent performance and white-light emission regulation through doping Eu^{3+}/Tb^{3+}, Appl. Organomet. Chem. 34 (2020) https://doi.org/10.1002/aoc.5506.

[4] K. Subodh, Prakash, K. Chaudhary, D.T. Masram, A new triazine-cored covalent organic polymer for catalytic applications, Appl. Catal. Gen. 593 (2020), https://doi.org/10.1016/j.apcata.2020.117411.

[5] G. Li, X. Zhou, Z. Wang, Highly nitrogen-rich microporous polyaminals using N, N-dimethylformamide and formamide as the starting monomers for CO_2 adsorption and separation, J. Phys. Chem. C 124 (2020) 3087–3094, https://doi.org/10.1021/acs.jpcc.9b10590.

[6] Y.-J. Ma, J.-X. Hu, S.-D. Han, J. Pan, J.-H. Li, G.-M. Wang, Manipulating on/off single-molecule magnet behavior in a Dy(III)-Based photochromic complex, J. Am. Chem. Soc. 142 (2020) 2682–2689, https://doi.org/10.1021/jacs.9b13461.

[7] D. Utreja, J. Kaur, K. Kaur, P. Jain, Recent advances in 1,3,5-triazine derivatives as antibacterial agents, Mini Rev Org Chem 17 (2020) 991–1041, https://doi.org/10.2174/1570193X17666200129094032.

[8] S. Noureen, S. Ali, J. Iqbal, M.A. Zia, T. Hussain, Synthesis, comparative theoretical and experimental characterization of some new 1,3,5 triazine based heterocyclic compounds and in vitro evaluation as promising biologically active agents, J. Mol. Struct. 1268 (2022) 133622, https://doi.org/10.1016/J.MOLSTRUC.2022.133622.

[9] A. Kajal, S. Bala, S. Kamboj, N. Sharma, V. Saini, Schiff bases: a versatile pharmacophore, Journal of Catalysts (2013) 1–14, https://doi.org/10.1155/2013/893512, 2013.

[10] P. Goel, D. Kumar, S. Chandra, Schiff`s base ligands and their transition metal complexes as antimicrobial agents, J. Chem. Bio. Phy. Sci. Section A. 4 (2014) 1946–1964.

[11] S.Y. Ebrahimipour, M. Khosravan, J. White, S. Fekri, Preparation, crystal structure, spectroscopic studies, DFT calculations, antibacterial activities and molecular docking of a tridentate Schiff base ligand and its cis-MoO2 complex, Appl. Organomet. Chem. 32 (2018) e4233, https://doi.org/10.1002/aoc.4233.

[12] O.S. Senturk, S. Sert, Synthesis and characterization of metal carbonyls [M(CO) 6 (M = Cr, Mo, W), Re(CO) 5 Br, Mn(CO) 3 Cp] with 2-Hydroxy-1-napthal-dehyde ethanesulfonylhydrazone (nafesh), Z. Naturforsch. 58 (2003) 1124–1127.

[13] M. V V, S. Pola, P. Chetti, Optoelectronic and charge transport properties of D-n-A type 1,3,5-triazine derivatives: a combined experimental and DFT study, Spectrochim. Acta Mol. Biomol. Spectrosc. 245 (2021) 118940, https://doi.org/10.1016/J.SAA.2020.118940.

[14] M.S. Polzella, P. Lodeyro, Re-evaluating semi-empirical computer simulations in quantum chemistry, Found. Chem. 21 (2019) 83–95, https://doi.org/10.1007/s10698-018-09329-w.

[15] H.H. Monfared, O. Pouralimardan, C. Janiak, Synthesis and spectral characterization of hydrazone Schiff bases derived from 2,4-dinitrophenylhydrazine, Crystal Structure of Salicylaldehyde-2,4-Dinitrophenylhydrazone 62 (2007) 717–720. http://znaturforsch.com. (Accessed 17 June 2023).

[16] H. Möhrle, G. Keller, α-Dicarbonylmonohydrazone und ihre Acylderivate als Nucleophile und Nachbargruppen α-Dicarbonylmonohydrazones and their Acylderivatives as Nucleophiles and Neighbouring Groups, Z. Naturforsch. 58 (2003) 885–902. http://znaturforsch.com. (Accessed 17 June 2023).

[17] J. Chakraborty, R.K.B. Singh, B. Samanta, R. Choudhury, S.K. Dey, P. Talukder, M.J. Borah, S. Mitra, Two new quadridentate Schiff base complexes of nickel(II) and cobalt(III): synthesis, structure and spectral characterisation, Z. Naturforsch. 61 (2006) 1209–1216. http://znaturforsch.com. (Accessed 17 June 2023).

[18] D. Enders, H. Schubert, C. Nübling, Enantioselective synthesis of α-substituted primary amines by nucleophilic addition to aldehyde-SAMP hydrazones, Angew Chem. Int. Ed. Engl. 25 (1986) 1109–1110, https://doi.org/10.1002/anie.198611091.

[19] D. Perdicchia, E. Licandro, S. Maiorana, C. Baldoli, C. Giannini, A new 'one-pot' synthesis of hydrazides by reduction of hydrazones, Tetrahedron 59 (2003) 7733–7742, https://doi.org/10.1016/S0040-4020(03)01208-0.

[20] M. Katyal, Y. Dutt, Analytical applications of hydrazones, Talanta 22 (1975) 151–166, https://doi.org/10.1016/0039-9140(75)80161-5.

[21] D.G. Carroll, L.G. Vanquickenborne, S.P. McGlynn, Semiempirical molecular orbital calculations. II. The nonbonding orbital, the electronic spectrum, and the spin—orbit coupling in X2CO molecules, J. Chem. Phys. 45 (1966) 2777–2784, https://doi.org/10.1063/1.1728025.

[22] M. Pandeeswaran, E.H. El-Mossalamy, K.P. Elango, Spectroscopic studies on the interaction of cilostazole with iodine and 2,3-dichloro-5,6-dicyanobenzoquinone, Spectrochim. Acta Mol. Biomol. Spectrosc. 78 (2011) 375–382, https://doi.org/10.1016/J.SAA.2010.10.023.

[23] S.M. Ahmed, I.A. Shaaban, E.H. El-Mossalamy, T.A. Mohamed, Synthesis, conformational analysis, infrared, Raman and UV-visible spectra of novel Schiff bases compiled with DFT calculations, Comb. Chem. High Throughput Screen. 23 (2020) 568–586, https://doi.org/10.2174/1386207323666200127161207.

[24] M.E. Moustafa, E.H. EL-Mossalamy, A.S. Amin, Synthesis and efficiency of 5-(2-hydroxyphenylazo)-indazoles as new reagents for the determination of vanadium, Monatshefte Für Chemie Chemical Monthly 126 (1995) 901–908, https://doi.org/10.1007/BF00811009.

[25] H. Khanmohammadi, M.H. Abnosi, A. Hosseinzadeh, M. Erfantalab, Synthesis, biological and computational study of new Schiff base hydrazones bearing 3-(4-pyridine)-5-mercapto-1,2,4-triazole moiety, Spectrochim. Acta Mol. Biomol. Spectrosc. 71 (2008) 1474–1480, https://doi.org/10.1016/j.saa.2008.05.003.

[26] E.H. El-Mossalamy, Molecular spectroscopic studies of charge transfer complexes of thiourea derivatives with benzoquinones, J. Mol. Liq. 123 (2006) 118–123, https://doi.org/10.1016/j.molliq.2005.07.003.

[27] R.M. Silverstein, F. Webster, D. Kiemle, Spectrometric identification of organic compounds, 7ed 2005 – silverstein, webster & kiemle, Microchem. J. 21 (2005).

[28] T. Lu, F. Chen, Multiwfn: a multifunctional wavefunction analyzer, J. Comput. Chem. 33 (2012) 580–592, https://doi.org/10.1002/jcc.22885.

[29] R.A. Gaussian, 1, mj frisch, gw trucks, hb schlegel, ge scuseria, ma robb, jr cheeseman, g. Scalmani, v. Barone, b. Mennucci, ga petersson et al, gaussian, Inc., Wallingford CT 121 (2009) 150–166.

[30] Y.Y. Lin, N.P. Rajesh, P. Santhana Raghavan, P. Ramasamy, Y.C. Huang, Crystal growth of two-component new novel organic NLO crystals, Mater. Lett. 56 (2002) 1074–1077, https://doi.org/10.1016/S0167-577X(02)00680-8.

[31] E.-S. El-Mossalamy, N. Wazzan, L. Alharbi, DFT calculations of charge transfer complexes of ....Thiourea and benzoquinines, Asian J. Chem. 27 (11) (2015) 3937–3950.

[32] Y.M. Issa, S.A. Abdel-Latif, A.L. El-Ansary, H.B. Hassib, The synthesis, spectroscopic characterization, DFT/TD-DFT/PCM calculations of the molecular structure and NBO of the novel charge-transfer complexes of pyrazine Schiff base derivatives with aromatic nitro compounds, New J. Chem. 45 (2021) 1482–1499, https://doi.org/10.1039/D0NJ05397J.

[33] S. Singh, M.K. Mandal, A. Masih, A. Saha, S.K. Ghosh, H.R. Bhat, U.P. Singh, 1,3,5-Triazine: a versatile pharmacophore with diverse biological activities, Arch. Pharm. (Weinheim) 354 (2021) 2000363, https://doi.org/10.1002/ardp.202000363.

[34] C. Zhou, J. Min, Z. Liu, A. Young, H. Deshazer, T. Gao, Y.-T. Chang, N.R. Kallenbach, Synthesis and biological evaluation of novel 1,3,5-triazine derivatives as antimicrobial agents, Bioorg Med Chem Lett 18 (2008) 1308–1311, https://doi.org/10.1016/j.bmcl.2008.01.031.

[35] D. Liu, P. Guo, C. McCarthy, B. Wang, Y. Tao, D. Auguste, Peptide density targets and impedes triple negative breast cancer metastasis, Nat. Commun. 9 (2018) 2612, https://doi.org/10.1038/s41467-018-05035-5.

[36] A. Wróbel, B. Kolesińska, J. Frączyk, Z.J. Kamiński, A. Tankiewicz-Kwedlo, J. Hermanowicz, R. Czarnomysy, D. Maliszewski, D. Drozdowska, Synthesis and cellular effects of novel 1,3,5-triazine derivatives in DLD and Ht-29 human colon cancer cell lines, Invest New Drugs 38 (2020) 990–1002, https://doi.org/10.1007/s10637-019-00838-9.

[37] M. Khalili, A. Rahimi-Movaghar, B. Shadloo, R. Mojtabai, K. Mann, M. Amin-Esmaeili, Global scientific production on illicit drug addiction: a two-decade analysis, Eur Addict Res 24 (2018) 60–70, https://doi.org/10.1159/000487590.

[38] D. Maliszewski, D. Drozdowska, Recent advances in the biological activity of s-triazine core compounds, Pharmaceuticals 15 (2022) 221, https://doi.org/10.3390/ph15020221.

[39] K.M.Z. Hossain, U. Patel, I. Ahmed, Development of microspheres for biomedical applications: a review, Prog Biomater 4 (2015) 1–19, https://doi.org/10.1007/s40204-014-0033-8.